AREVA

September 22, 2010
NRC:10:087

Document Control Desk
U.S. Nuclear Regulatory Commission
Washington, D.C. 20555-0001

Response to U.S. EPR Design Certification Application RAI No. 339, Supplement 7

Ref. 1: E-mail, Getachew Tesfaye (NRC) to Ronda Pederson, et al (AREVA NP Inc.), "U.S. EPR Design Certification Application RAI No. 349 (4164, 4165), FSAR Ch. 19 OPEN ITEM," January 8, 2010.

Ref. 2: E-mail, Martin Bryan (AREVA NP Inc.) to Getachew Tesfaye (NRC) " Response to U.S. EPR Design Certification Application RAI No. 349, FSAR Ch. 19 OPEN ITEM, Supplement 2, Supplement 1," April 30, 2010.

Ref. 3: E-mail, Martin Bryan (AREVA NP Inc.) to Getachew Tesfaye (NRC) " Response to U.S. EPR Design Certification Application RAI No. 349, FSAR Ch. 19 OPEN ITEM, Supplement 3," May 24, 2010.

In Reference 1, the NRC provided a request for additional information (RAI) regarding the U.S. EPR design certification application (i.e., RAI No. 349). A schedule for responding to this RAI was provided in Reference 3. In Reference 2 AREVA NP submitted Supplement 2 to the response to provide technically correct and complete responses to 2 of the 6 questions. Supplements 4 through 6 provided a revised schedule for the remaining 4 questions. Technically correct and complete responses to 2 of the remaining 4 questions in RAI No. 349 are enclosed with this letter.

Appended to the enclosure are affected pages of the U.S. EPR Final Safety Analysis Report in redline-strikeout format which support the response to RAI 349 Question 19-333.

The enclosed response consists of the following:

Question #	Start Page	End Page
RAI 349 — 19-332	2	57
RAI 349 — 19-333	58	65

AREVA NP considers some of the material contained in the enclosure to be proprietary. As required by 10 CFR 2.390(b), an affidavit is enclosed to support the withholding of the information from public disclosure. Proprietary and non-proprietary versions of the enclosure to this letter are provided.

The schedule for the two remaining questions is being revised to allow more time for NRC interaction on the responses.

D077
NRO

The schedule for technically correct and complete responses to the 2 remaining questions has been changed and is provided below:

Question #	Response Date
RAI 349 — 19-334	October 27, 2010
RAI 349 — 19-335	October 27, 2010

If you have any questions related to this submittal, please contact me by telephone at 434-832-2369 or by e-mail at sandra.sloan@areva.com.

Sincerely,

Sandra M. Sloan, Manager
New Plants Regulatory Affairs
AREVA NP Inc.

Enclosures

cc: G. Tesfaye
Docket No. 52-020

AFFIDAVIT

COMMONWEALTH OF VIRGINIA)
) ss.
CITY OF LYNCHBURG)

1. My name is George Pannell. I am Manager, Regulatory Affairs for AREVA NP Inc. and as such I am authorized to execute this Affidavit.

2. I am familiar with the criteria applied by AREVA NP to determine whether certain AREVA NP information is proprietary. I am familiar with the policies established by AREVA NP to ensure the proper application of these criteria.

3. I am familiar with the AREVA NP information contained in the draft response "Response to Request for Additional Information No. 349, Supplement 7" and referred to herein as "Document." Information contained in this Document has been classified by AREVA NP as proprietary in accordance with the policies established by AREVA NP for the control and protection of proprietary and confidential information.

4. This Document contains information of a proprietary and confidential nature and is of the type customarily held in confidence by AREVA NP and not made available to the public. Based on my experience, I am aware that other companies regard information of the kind contained in this Document as proprietary and confidential.

5. This Document has been made available to the U.S. Nuclear Regulatory Commission in confidence with the request that the information contained in this Document be withheld from public disclosure. The request for withholding of proprietary information is made in accordance with 10 CFR 2.390. The information for which withholding from disclosure is

requested qualifies under 10 CFR 2.390(a)(4) "Trade secrets and commercial or financial information".

6. The following criteria are customarily applied by AREVA NP to determine whether information should be classified as proprietary:

(a) The information reveals details of AREVA NP's research and development plans and programs or their results.

(b) Use of the information by a competitor would permit the competitor to significantly reduce its expenditures, in time or resources, to design, produce, or market a similar product or service.

(c) The information includes test data or analytical techniques concerning a process, methodology, or component, the application of which results in a competitive advantage for AREVA NP.

(d) The information reveals certain distinguishing aspects of a process, methodology, or component, the exclusive use of which provides a competitive advantage for AREVA NP in product optimization or marketability.

(e) The information is vital to a competitive advantage held by AREVA NP, would be helpful to competitors to AREVA NP, and would likely cause substantial harm to the competitive position of AREVA NP.

The information in the Document is considered proprietary for the reasons set forth in paragraph 6(d) above.

7. In accordance with AREVA NP's policies governing the protection and control of information, proprietary information contained in this Document has been made available, on a limited basis, to others outside AREVA NP only as required and under suitable agreement providing for nondisclosure and limited use of the information.

8. AREVA NP policy requires that proprietary information be kept in a secured file or area and distributed on a need-to-know basis.

9. The foregoing statements are true and correct to the best of my knowledge, information, and belief.

SUBSCRIBED before me this
21st day of September 2010.

Sherry L McFaden
NOTARY PUBLIC, COMMONWEALTH OF VIRGINIA
MY COMMISSION EXPIRES: 10/31/10
Reg. # 7079129

SHERRY L. MCFADEN
Notary Public
Commonwealth of Virginia
7079129
My Commission Expires Oct 31, 2010

Response to

Request for Additional Information No. 349, Supplement 7

01/26/2010

U. S. EPR Standard Design Certification
AREVA NP Inc.
Docket No. 52-020
SRP Section: 19 - Probabilistic Risk Assessment and Severe Accident Evaluation
Application Section: FSAR Chapter 19

QUESTIONS for PRA Licensing, Operations Support and Maintenance Branch 2 (ESBWR/ABWR Projects) (SPLB)

Question 19-332:

OPEN ITEM

Follow-up to RAI No. 236, Question 19-312

The responses to the various questions listed as part of the subject RAI were for the most part satisfactory. In several areas, however, the information provided is insufficient for developing sufficient confidence that the integrity of the proposed material for the U.S. EPR reactor pit can be maintained during potential severe accidents.

Further clarification is requires, as follows:

a) The information provided on the material characteristics of the stabilized ZrO_2 does not include the solidus temperature of the U.S. EPR-specific MgO-stabilized Zirconia. Please provide the solidus temperature of Zettral 95GR that is planned to be installed in the U.S. EPR reactor pit.

b) The MgO-stabilized ZrO_2-tested for compatibility with metallic melts was found to be stable to 2200°C for duration of six hours under relatively oxygen-free melt condition. However, it was mentioned that melt infiltration (but no significant thinning) of the ceramics was observed for oxygen contents higher than postulated for U.S. EPR severe accident melts. Please provide justification by presenting available experimental evidence on the compatibility of U.S. EPR specific zirconia (or similar zirconia) with metallic melts having oxygen contents in the range expected for severe accidents in the U.S. EPR.

c) A summary of data on thermal up-shock experiments with molten iron from thermite reaction with U.S EPR-specific Zettral 95GR bricks and the refractory mortar between the bricks, was indicated to show that the bricks and associated mortar survived without significant damage thermal-up shock caused by pouring molten iron from thermite reaction onto the bricks. Please provide the measured temperature-time histories in the Zettral 95GR bricks for the thermal up-shock experiments. Show a comparison of the measured parameters to predictions under severe accident conditions in the U.S. EPR. In addition, provide a comparison of melt impact velocities and mass of melt arrival per unit area of zirconia per unit time in the experiments to predictions under typical severe accidents in the U.S. EPR.

d) A summary of experiments on the interaction of oxidic melts with ZrO_2, including Zettral 95 GR sample materials (not bricks) under MCCI conditions are stated to show that the zirconia samples survived with minimal attack because, it is asserted, the MCCI causes the addition of low-melting concrete decomposition products into the corium melt, thus keeping the melt temperature below the liquidus, and causes the melt to be saturated with zirconia. The interaction time between the melt and the ZrO_2 varied from 5 to 15 minutes for the four experiments. This time range is small compared with the estimated time of 3 hours for retention of the melt in the reactor pit. Reference is also made to the MACE experiments. Please provide experimental evidence (e.g., AREVA, MACE, etc.) on the time evolution of melt temperatures during sustained tests, including MCCI, supporting the compatibility oxidic melts with Zirconia.

e) A discussion of the "adapted" microstructure of Zettral 95GR was provided, in which features such as granular structure, internal microscopic cracks, thermal strain of texture, expansion of sintering bridges, formation of collective pores, and curing of micro cracks are described. Also, the discussion of the mechanical behavior of Zettral 95GR is inscrutable without further explanation. Please provide a more precise description of what is meant by the "adapted" microstructure of Zettral 95GR. Furthermore, provide a more clear discussion of the wedge splitting test, how crack openings (strains) in the range 1E-5 to 1E-4 are derived, and provide a description of the material transfer forces in the presence of such cracks.

Response to Question 19-332:

Zirconia-based protective material is used in the U.S. EPR core melt stabilization system (CMSS) to prevent uncontrolled interaction of the molten corium with the structural concrete. The highest corresponding risk exists:

- During the initial period of temporary retention in the pit.
  Without a protective layer, the extent of local radial erosion is unpredictable and an attack on the structural concrete behind the sacrificial concrete is possible. This is true in case of a stratified melt configuration while the molten metallic phase is less dense and on top of the oxidic phase (before layer inversion). The upwards heat flux from the oxide layer could then be focused by the metallic layer into the surrounding cylindrical sidewall similar to the case of in vessel retention. Corresponding radial heat fluxes and concrete erosion rates could be high. The protective zirconia layer, which is stable against the attack of the steel melt under these conditions, avoids erosion. The risk of fast progression in the oxidic melt region is comparably smaller because of lower heat fluxes.
- During melt release into the melt discharge channel.
  The zirconia layer insulates the concrete that surrounds the channel and withstands the thermal shock of the impacting melt during the time of melt release through the gate. The zirconia material should preserve its integrity under the developing thermal stress conditions to avoid a progressive failure. This requirement has been considered early in the selection of the material and resulted in a zirconia brick of high porosity and correspondingly high "elasticity" under thermal stress. The case of oxide melt release is less critical because an impacting oxidic melt forms thin crusts on either the steel plate located on top of the zirconia, or on the initially cold refractory material itself. Such crusts establish thermal resistances and reduce the thermal-up shock.

Response to Question 19-332, Part a:

RHI, the material supplier for Zettral 95GR, identifies the chemical composition of Zettral 95GR (in wt%) as 93 percent ZrO_2, 4.0 percent MgO, 1.9 percent SiO_2, 0.8 percent Al_2O_3, 0.2 percent CaO, 0.5 percent Fe_2O_3, and 0.2 percent TiO_2. The chemical composition of Zettral 95GR has a density of 4.4 g/cm^3 and a porosity of 18.5 vol%.

A "solidus temperature" of zirconia Zettral 95GR is not a relevant parameter for the application. The main "impurity" in Zettral 95GR is MgO, with a concentration of 4 wt% or 11.4 mol% MgO. It is used to partially stabilize the cubic ZrO_2 modification. The phase diagram of ZrO_2-MgO in Figure 19-332-1 shows that the solidus temperature at 11 to 12 mol% MgO is above 2500°C. Other oxides are present in a minimal concentration, and do not exist as separate oxides but form high-melting compounds such as fosterite ($2MgO \cdot SiO_2$) or spinel phases.

The results of testing with metal and oxidic melt confirmed that the application temperature ("operating temperature") of partially stabilized zirconia is higher than the melt temperatures. For metal melts, temperatures were 1900 to 2200°C (see part 19-332b of this response), and for oxide melts, initial temperatures in molten corium-to-concrete interaction (MCCI) tests were 2200 to 2300°C (see part 19-332d of this response).

AREVA NP metal melts testing used zirconia crucibles made of sintered material (composition #3001 and #3004, ZIRCOA Solon Ohio). These materials contain similar concentrations of low-melting oxides as Zettral 95GR. For example, the ZIRCOA datasheet on composition #3001 identifies it as 94.7 wt% ZrO_2, 2.6 wt% MgO, 1.5 wt% SiO_2, 0.8 wt% $Al2O_3$, 0.2 wt% CaO, 0.1 wt% Fe_2O_3, and 0.1 wt% TiO_2 with a density 4.6 g/cm^3 and porosity 18 vol%.

Iron and steel melts in crucibles of these materials were heated up to 1800 to 2200°C and kept at the maximum temperature for several hours. No melt phases were observed.

For example, in one test a steel melt (88 wt% Fe, 5 wt% Cr, 7 wt% Ni) containing little dissolved oxygen was kept in a crucible of #3001 material at 2200°C for six hours. The sintered zirconia remained stable throughout the test and kept its initial geometry. The RAI 236, Supplement 2, Response to Question 19-312 and the Response to Question 19-332b provide detailed tests and results.

In other tests, steel melts with the same composition with conservative oxygen concentrations up to the saturation limit in (88 wt% Fe, 5 wt% Cr, 7 wt% Ni) kept in #3001 crucibles were heated up to 1900°C for three hours. The deoxidant chromium limits saturation with oxygen to typical U.S. EPR concentrations to below 0.2 wt% O (see part 19-332b of this response). Under these conditions, no melt phases were observed.

Higher melt temperatures were applied to zirconia #3004 (supplied by ZIRCOA) in the CIRMAT experiments using oxidic melts discussed further in Annex to Part a. The CIRMAT tests investigated the dissolution of sintered zirconia ceramic by superheated prototypic corium melts at high temperatures (2550 to 2850°C). The UO_2-ZrO_2 and UO_2-ZrO_2-Zr melts were superheated by up to 260K (i.e., up to 260K above their liquidus temperature). Durations of interaction ranged from 21 to 250 minutes. After ablation of some zirconia into the superheated melt, a second steady-state phase followed where no more ablation occurred. During the second phase, the top of the material still experienced high temperatures from the sustained-heated melt. The height of the zirconia brick material remained unchanged, which indicates high temperature resistance. Figure 19-332-2 shows the test specimen after interaction with the oxidic melt.

In the application case, the dimension inside the brick at high temperature is relatively small because of low thermal conductivity of zirconia. The temperature gradient inside zirconia bricks was calculated. The dimension with temperatures exceeding 1900°C or 1500°C increases in time but is still small relative to 20cm length of the zirconia brick. In the RAI 236, Supplement 2, Response to Question 19-312, the calculated temperature profiles inside a 20cm thick zirconia brick layer were shown (see Figure 19-312-2). Contact temperatures on the zirconia melt-side were assumed to be 2200 to 2300°C and lasted for three hours. Due to the low thermal conductivity of zirconia, 15cm of the zirconia brick still were below 1500°C, even after the conservatively long time span of three hours.

Annex to Part a:

Summary or CIRMAT Tests (zirconia brick material, composition #3004, ZIRCOA)

Behavior of ZrO2 in Contact with Superheated Oxidic Melts

Superheated oxidic melts are not relevant for the U.S. EPR melt retention. To fill specific knowledge gaps, the behavior of zirconia ceramic in superheated oxidic melts was studied.

UO2-ZrO2-Zr Melts (CIRMAT Laboratory Tests)

In the CIRMAT tests, cylindrical ZrO_2 specimen made from zirconia bricks (partially stabilized by MgO, composition #3004, ZIRCOA) were placed underneath a superheated oxidic melt and their dissolution behavior investigated.

The objectives of the CIRMAT tests were to determine the following:

- Time-dependent ablation rate of ZrO_2 ceramic in stoichiometric UO_2-ZrO_2 melts and in substoichiometric UO_2-ZrO_2-Zr melts.
- Effect of temperature (2450 to 2850°C) and Zr content on ZrO_2 ablation rate.

The tests were performed in a high-frequency cold crucible induction melter. In this process, the energy is transferred by induction directly into a ceramic melt, which is inside a crucible of the same material (a "skull" consisting of an approximately 2mm thick crust of the molten material that has solidified on the cold walls of water-cooled copper tubes). Convection is established in the melt, its intensity depending on the degree of superheat. The velocity on the surface of the melt was determined to be 40 to 80 mm/s using a video camera.

The results of the tests using stoichiometric UO_2-ZrO_2 melts (i.e., Zr-free melts) on immersion specimens and bottom specimens are presented in this response.

Cylindrical bottom specimens (composition #3004/ZIRCOA, diameter: 72.5 mm; height: 65 mm) were used. A 50mm high ceramic ring was placed between the ZrO_2 specimen and the water-cooled bottom of the crucible as an additional thermal insulator. The ZrO_2 ceramic was fitted with thin thermocouple wires at various heights close to the cylinder axis to measure the temperature time history inside the ZrO_2 and determine the ablation rate.

In the tests, two temporal phases can be observed in the case of the tests with the bottom specimens. An approximately linear ZrO_2 ablation curve is followed by a second phase in which ZrO_2 ablation proceeds at a rate of only 0.01 to 0.06 mm/minute (possibly because of melt saturated with ZrO_2).

For example, in Test #24, the ablation of ZrO_2 bottom specimens was investigated using a melt composed of 71 wt% UO_2 and 29 wt% ZrO_2. At a melt temperature of approximately 2550°C (low superheat), 11 mm of ZrO_2 was removed in 400 seconds. This corresponds to a mean ablation rate of 1.5 mm/minute. The total test duration was 31 minutes.

In comparison, at a melt superheat (T_{melt} - $T_{liquidus}$) of approximately 200 K, the ablation rate is about three times higher. For the U.S. EPR, a superheated melt is not relevant because the

oxidic melt in the reactor pit is always subcooled due to the MCCI process and saturated in the refractory compounds urania and zirconia.

Time-dependent temperature profiles were measured at various heights in the ceramic specimen during the tests.

The appearance of the specimen from Test #24 can be seen in Figure 19-332-3. The ZrO_2 cylinder with the milled slots for the thermocouple wires is in the center, with remains of the melt lying on top. In this and other specimens, cracks were found after rapid cooldown of the melt. These cracks did not penetrate through the material and may have arisen upon cooling (shrinkage cracks).

The interaction zone consists of several areas as illustrated in Figure 19-332-4. The total test duration was 30 minutes.

The subsequent ceramographic analysis revealed the following:

- Area I: molten ceramic, 0.3 to 0.5 mm thick.
- Area II: area with large grain size.
- Area III: formation of macropores and some cracks.
- Area IV (5 to 10 mm from hot end): black color; microstructure contains coarsened grains with pore fractions after long-duration tests (four hours).

Uranium was only found in Area I, and no diffusion took place into the underlying areas.

Response to Question 19-332, Part b:

In the U.S. EPR, iron oxide concentration (FeOx) in the oxide melt increases during melt retention in the pit from 0 wt% at 2350°C to 7 to 8 wt% at 2100°C (gate failure). In contact with the oxidic melt, oxygen is transferred to the metal melt, leading to (Fe, Cr, Ni)(O). The maximum concentration (O) of dissolved oxygen in (Fe, Cr, Ni)(O), which corresponds to 7 to 8 wt% FeO, is below the threshold for interaction with ZrO_2, leading to corrosion of the material or liquid phases.

Iron or steel melts can absorb oxygen. The surface tension of these melts is successively reduced to where infiltration of zirconia into pore channels of ceramics is possible. At a high concentration of dissolved oxygen (i.e., significantly above the (O) concentrations possible for U.S. EPR), this was observed experimentally. Under U.S. EPR conditions, the oxygen concentration in the steel melt is too low for infiltration to occur and has not been observed experimentally.

More detail together with experimental evidence is provided in this response.

Theoretical Considerations

In the U.S. EPR, after the reactor pressure vessel (RPV) failure, the initial metallic melt (Fe, Cr, Ni, Zr) does not contain oxygen due to oxidation with Zr. At this time, the oxidic melt (UO_2, ZrO_2, Zr) is sub-stoichiometric and reducing, and cannot provide oxygen for the metal melt.

Ablation of iron-oxide containing sacrificial concrete leads to oxidation of (metallic) Zr by FeOx. After Zr oxidation, iron oxide from sacrificial concrete leads to a gradual increase of FeOx in the oxidic melt and of the oxygen concentration (O) in the steel melt (Fe, Cr, Ni)(O). At the time of gate failure, the highest FeO concentration in the oxide melt is 7 to 8 wt%. Oxide melt and steel melt are in close contact, which allows oxygen exchange between the two melt phases.

The maximal oxygen concentration possible in the steel melt is calculated for 1800°C and 1900°C, the highest temperatures of the steel melt. In a first approximation, the oxygen-diminishing effect of the deoxidant Cr is conservatively neglected.

The maximum oxygen concentration $(O)_{max}$ in an iron melt arises when covered with a pure FeO slag (oxide melt = 100 percent FeO). It changes with temperature according to Reference 2:

$\log (\%O)_{max} = - 6320 / T + 2.734.$

$(\%O)_{max}$ maximum oxygen concentration in a Fe melt covered by FeO slag (wt%).

T Temperature (K).

The maximum oxygen concentration $(O)_{max}$ using the equation in Reference 2 is 0.49 wt% at 1800°C and 0.67 wt% at 1900°C.

The maximum FeO concentration in the oxide melt is 7 wt% or approximately 12 mole%. Assuming ideal behavior of FeO, the maximum oxygen concentration in an iron melt covered by this oxide melt is about a factor of seven lower. Assuming ideal behavior, it is estimated that $(O)_{max} \approx 0.07$ wt% at 1800°C, and $(O)_{max} \approx 0.1$ wt% at 1900°C.

The deoxidant Cr, which decreases high oxygen concentrations and keeps them at a low limit, is considered. At high FeO concentrations in the oxidic melt and corresponding higher oxygen concentration in the steel melt, the deoxidant Cr is beneficial for the stability of the ZrO_2 protective layer.

The addition of iron oxide to the top slag of a steel melt leads to partial reduction of FeO to Fe and oxidation of Cr to Cr_2O_3. Reference 2 and Reference 3, which discuss metallurgy, show that FeO and Cr may coexist. For example, Figure 19-332-5 shows that 0.03-0.04 w% oxygen can be dissolved in a Fe/2-15 w% Cr melt at 1600°C. This oxygen amount is stable against Cr and is not oxidized to Cr_2O_3.

Industrial experiences in steel metallurgy reveal that a certain amount of metallic Cr remains in the steel melt. This is due to a chemical equilibrium between Fe, Cr and FeO, and Cr_2O_3. Cr is not quantitatively oxidized to Cr_2O_3 before oxidation of Fe in the steel melt takes place, but Cr and Fe oxidation are a simultaneous process (Cr is oxidized to a larger extent than Fe).

Assuming a conservatively low Cr concentration of 3 wt% in the steel melt (Fe, Cr, Ni), the oxygen activity a_O was calculated according to Reference 4:

$$\log K = \log ([\%Cr]^{0.5} a_O) = - \frac{12690}{T} + 5.41$$

K equilibrium constant (no dimension).

(%Cr) Cr concentration (wt%).

a_0 oxygen activity (wt%).

T Temperature (K).

The (maximum) oxygen activity a_O is 0.11 wt% at 1800°C and 0.21 wt% at 1900°C.

This result is beneficial for zirconia stability. The oxygen concentration in an iron melt covered by a slag containing 7 wt% FeO is lower than the oxygen activity in (Fe, 3 wt% Cr, Ni) melt: at 1800°C 0.7 wt% versus 0.11 wt% O and at 1900°C 0.1 wt% versus 0.21 wt% O. At (conservatively low) 3 wt% Cr, the desoxidizing effect is not necessary because the FeO content in the oxide melt is already low enough.

The physico-chemical concept of "virtual iron oxide activity" and its application to demonstrate chemical stability of zirconia against superheated iron and steel melts was discussed in the RAI 236, Supplement 2, Response to Question 19-312.

Experimental Results

[
]

The experimental results agree with the theoretical assessment described in this response, and zirconia ceramic is stable against steel melts under U.S. EPR conditions.

Response to Question 19-332, Part c:

Response to Question c-1: Measured data

General Remark:

Ceramic materials react brittle compared to metals when material is exposed to rapid stress changes. This effect is related to the kind of crystallografic stucture and type of chemical bonding of ceramics. The resistance to thermal shock can be influenced and improved by the macroscopic structure of the ceramic material. The grain size and the porosity (size, distribution) are proper instruments to match the thermal shock resistance requirements.

Coarse-grained material with relativly high porosity (e.g., 15 to 20 vol.-%) exhibit better thermal shock resistance than material sintered to maximum density.

Partly stabilized ZrO_2 has better fracture toughness than unstabilized ZrO_2 The toughness of stabilized zirconia can be attributed to some percentage of the structure going through the tetragonal-to-monoclinic transformation when stress is applied. The volume expansion that accompanies this transformation occurs at the tip of the crack and changes the stress field at the tip of the crack, reduces the rate of crack propagation, and improves its fracture toughness.

Experimental Evidence:

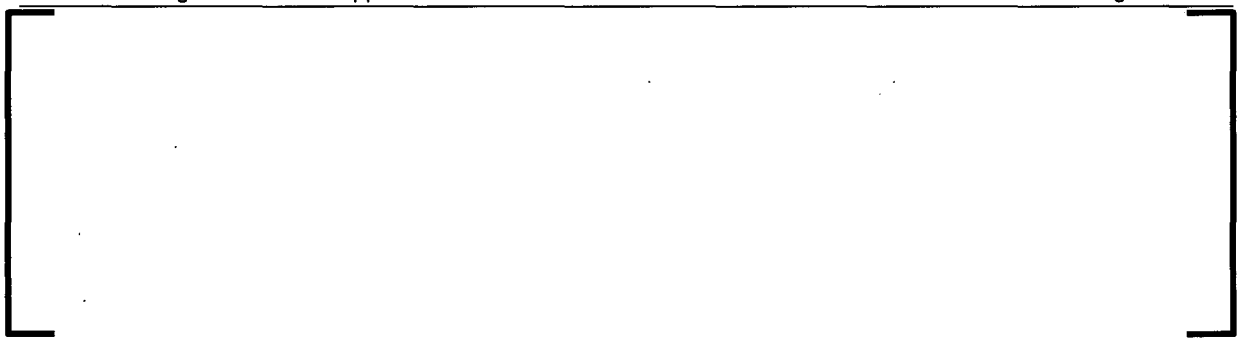

Response to Questions c-2 and c-3: Interpretation and Comparison

A comparison of experimental temperatures with predictions for the U.S. EPR protective zirconia is given in this response. Experimental temperature-time history corresponds to the one calculated for the U.S. EPR.

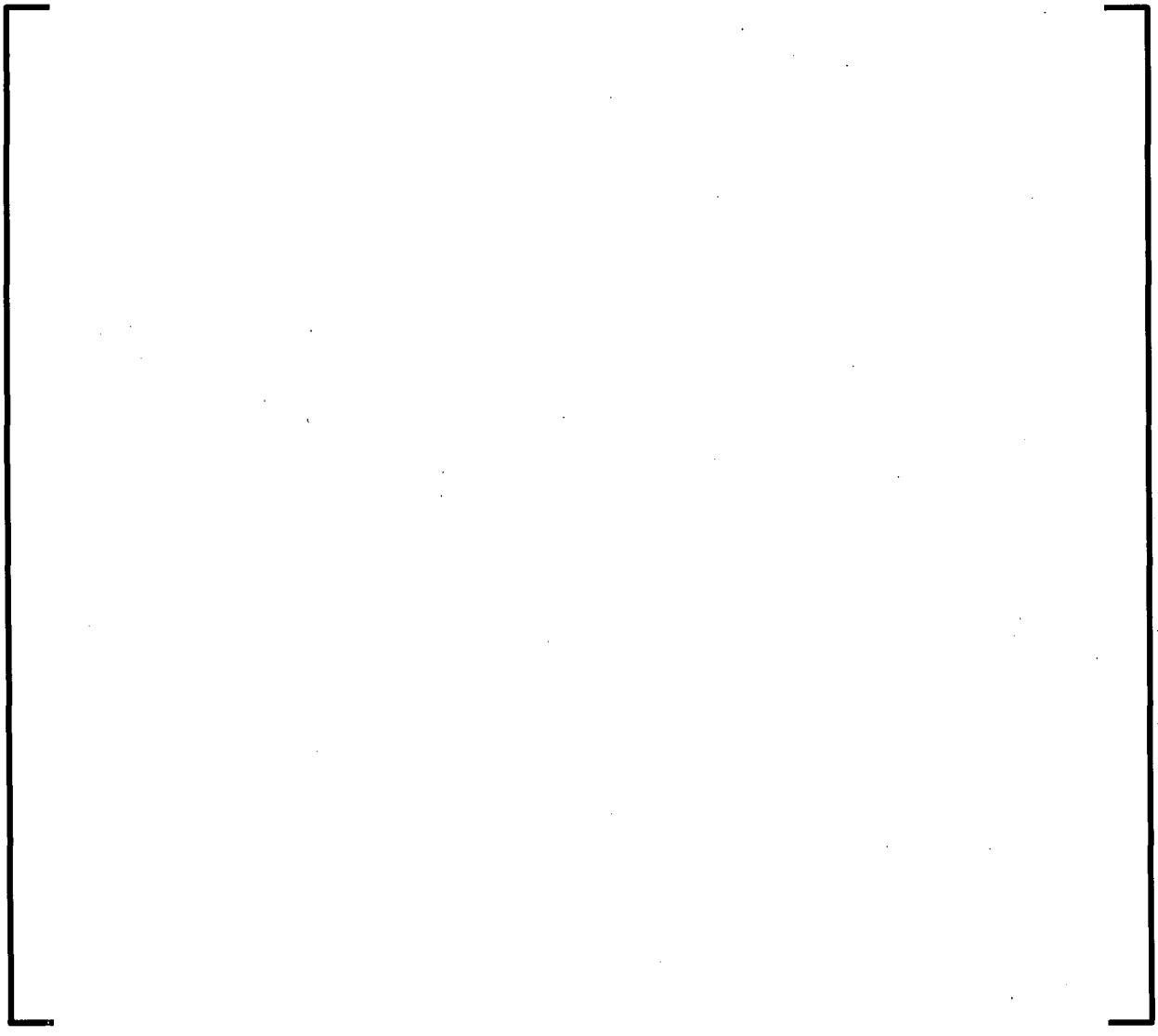

Addition to (c-3) from Material Point of View:

General Comment

Zirconia has a high mechanical stability as demonstrated by compression tests (cold compressive strength 110 N/mm^2). The mechanical impact is not a concern because in large-scale industry furnaces, the mechanical load on zirconia bricks at the lower side is high.

The stability towards thermal-up shock, which was tested under harsh conditions (sudden metallic melt contact without temperature attenuation due to a residual concrete layer), is the focus of this study.

Specific Answer

Total time of melt impact onto the bricks in the transfer channel is limited to five minutes. During these five minutes, only a small top layer of zirconia is heated up. The material below is "cold", and its mechanical stability is practically unchanged and capable of enduring high mechanical force.

From the behavior of Zettral 95GR against thermal shock, it is inferred that there is no crack formation at the surface. Even if it is conservatively assumed that a surface crack occurs, there are no consequences for brick assembly integrity. For this crack, it is not possible to open and be ajar. The brick is tied positively (force-fit) in the interlocked bracing system of the bricks, and the temperature in the brick top part is higher than in the lower parts. The resulting expansion forces lead to, at least partially, closure of the crack. When the melt in the crack is sufficiently cooled by the brick, it solidifies.

Response to Question 19-332, Part d:

General Comment

In the case of a melt pool with ongoing MCCI, the permanent addition of "cold" concrete decomposition products during MCCI absorbs energy from the melt. As shown in lab-scale experiments (see the RAI 236, Supplement 2, Response to Question 19-312), this leads to the formation of a sub-cooled melt, which agrees with the predictions. The temperature of such a melt is lower than its liquidus temperature. This sub-cooled, two-phase type of melt is

composed of a dispersed solid phase, mainly consisting of high-melting refractory components, and a liquid phase, mainly consisting of low melting concrete decomposition products. The melt is "saturated" in the refractory components zirconia and urania. Saturation of the melt with these components means that the driving force for chemical zirconia dissolution approaches zero. Consequently, the dissolution of zirconia ceases.

Based on this reasoning, the inert sidewalls in the MACE/MCCI-OECD large-scale tests were protected by a layer consisting of a refractory component of the melt (see References 7 and 8). ANL used urania instead of zirconia because the latter has a high electrical conductivity and would interfere with the electric heating method. Zirconia is equally stable under MCCI conditions, as both oxides are chemically similar. In the ANL tests, the inert side walls were never subject to a significant erosion or dissolution despite many hours of MCCI. The laboratory tests confirm this reasoning experimentally for zirconia. Ceramic zirconia samples were subjected to prototypic oxidic melts under MCCI conditions. The laboratory tests were carried out at AREVA NP, Erlangen, in the SICOPS facility, which uses a high frequency electromagnetic field for the generation and sustained heating of oxidic melts in a cold crucible.

The tests showed that the zirconia protective material is resistant to oxidic melts. In accordance with above conception of a melt saturated in refractory material, it was observed that no zirconia was dissolved in the melt. The stability is assigned to the MCCI process taking place in parallel and leading to a sub-cooled melt.

Concerning Time Evolution of Melt Temperatures during Sustained Tests

The temperature of the initially superheated melt (by approximately 100K, judging from pyrometer measurements) decreased after the onset of melt-concrete interaction, in the 1D tests within minutes.

The melt temperature was 50 to 100K below liquidus temperature during the MCCI process. Melt temperature in comparison to liquidus temperature measured in AREVA's own 1D MCCI tests is presented in Annex to Part d.

MCCI allows high convection in the melt pool due to gas release from the concrete. The temperature in the melt quickly equalizes.

Concerning the Duration of Zirconia Stability Tests under MCCI Conditions

In the tests, a zirconia dissolution rate of practically zero was found. After interaction, the samples had sharp edges or borders which confirm that there was no zirconia dissolution. No dissolution occurs at longer times. The "estimated time of three hours for retention of the melt in the reactor pit" is stated in context with a most conservative (here, highest) temperature load.

Test conditions were "harder" because in the application, only one side of the zirconia bricks is in contact with the melt. In the tests, the cylindrical zirconia samples, including Zettral 95GR, with 10mm diameter were successively surrounded by the oxidic melt. The zirconia top part experienced temperatures higher than if only one side had been heated for the same duration.

In the U.S. EPR case, the melt is definitively sub-cooled compared to its liquidus temperature. The sub-cooling is significantly higher than in the 1D zirconia stability tests. The iron oxide content in the melt does not exceed 7 to 8 wt% at the end of the retention phase. The erosive

conditions for the zirconia layer are milder in the application than in the laboratory tests. This provides an additional safety margin concerning protective material stability.

Reference to MACE Experiments

The use of a urania-pellet layer to protect the non-concrete sidewalls in the MACE experiments and the use of porous sintered zirconia behind the sacrificial concrete in the pit of the U.S. EPR is supported by the same logic, as explained in the following section.

During MCCI in the reactor pit, "cold" concrete decomposition products (gas and slag) are initially mixed into a molten corium pool that mainly consists of zirconia and urania. The concrete admixture changes the pools chemical composition, solidus-liquidus range, and temperature, and verifies that the mixture is sub-cooled. This is caused by the direct cooling effect and because for the wide solidus-liquidus range, the viscosity of the pool allows extraction of the internal decay power via gas-enhanced convection at high volumetric solid fractions of up to 30 percent to 40 percent.

The melt's solid phase consists of the core-oxides zirconia and urania. Because the core-oxides have a high density, a high percentage of the core-oxides can exists as solid crystallites in a liquid phase consisting of lower-melting concrete decomposition products without significantly increasing the viscosity of the pool. This allows low melt temperatures.

The dispersed mass represents a specific surface that is higher than the surrounding zirconia surface exposed to the melt. Whenever conditions exist which allow dissolution of more refractory species in the melt (e.g., after concrete dissolution), these species will come from the mass of dispersed solid particles. Zirconia (and urania) sidewalls are stable for the duration of the MCCI.

The MCCI pool temperature is determined by the content of concrete. In the early phases of the MCCI in the U.S. EPR pit, the concrete fraction is low and the solidus-liquidus range is narrow (<100K). At this time, pool-temperatures are predicted to be as high as approximately 2500°C. This early situation is not relevant for the stability of the protective layer, because the layer is not yet exposed to the melt.

A concrete mass fraction of about 10wt% is required to establish the reduction of the solidus temperature and the formation of a concrete-rich liquid phase, as observed in the MACE, the OECD-MCCI (CCI), and the VULCANO programs. This is achieved in the U.S. EPR after about 20 tons of concrete are mixed into the oxidic melt.

In these experiments, those with the highest MCCI temperatures (2200°C to 2100°C) were the MACE tests because these tests were 1D (erosion only in downward direction, four inert sidewalls, two with electrodes). During the test, pool temperatures (at constant power) decline steadily by the addition of concrete decomposition products. At some point in time, water was added at the surface, after which the melt entered into quenching transients, typically followed by the formation of a stable crust and smaller molten pools of different composition (less core oxides) and lower temperature.

Sample temperature plots from MACE tests M3b and M4 are shown in Figures 19-332-22 and 19-332-23.

In these tests, melt temperatures were above 2000°C over a significant period of time, often during several hours.

The assumption of a three hour contact period was made to generate bounding temperature for the structural concrete around the reactor pit. In reality, much shorter periods of melt-zirconia contact are expected.

Elements that guarantee the stability of the zirconia protective material in the U.S. EPR pit are the unique features of the MCCI pool described in this response, namely the sustained sub-cooling and a dispersed refractory phase of the same (or chemically similar) kind as the wall material itself.

Annex to Part d: Melt temperatures in 1-D MCCI tests

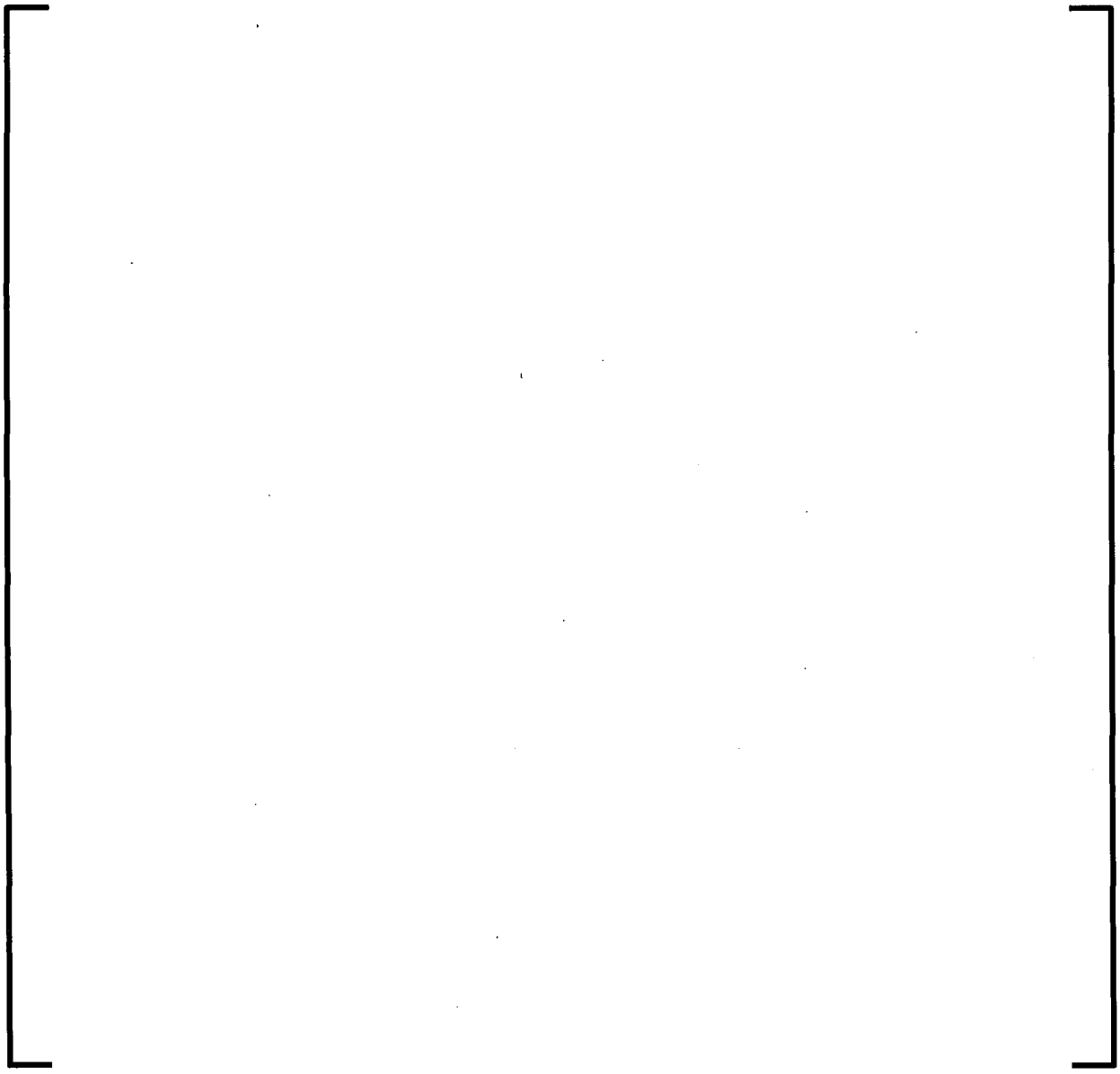

Test HTSC-Y´ (Simulant Melt, Concrete FESI-PZ15-8)

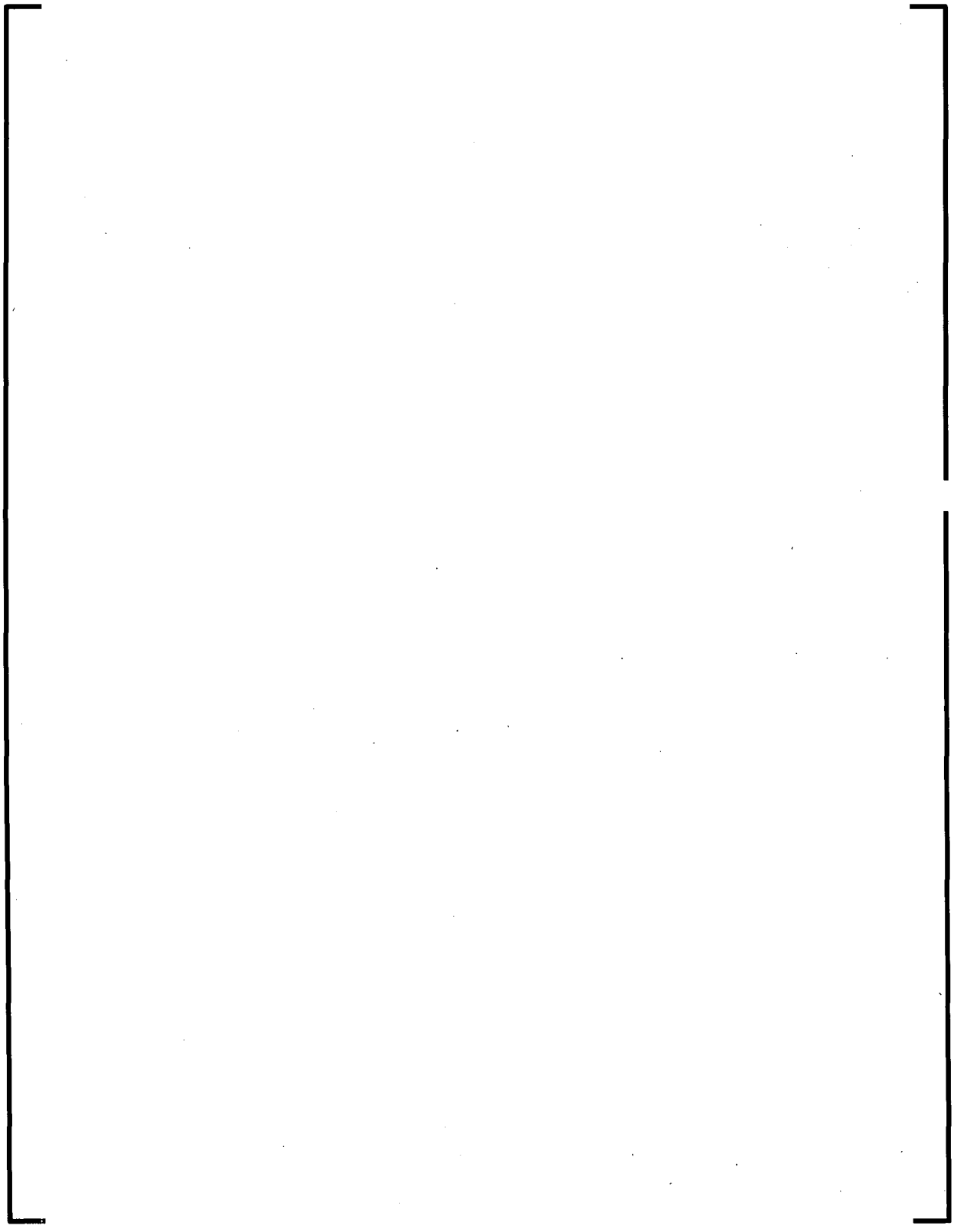

FSAR Impact:

The U.S. EPR FSAR will not be changed as a result of this question.

References for Question 19-332:

1. Levin, Ernest M., "Phase diagrams for ceramists", The American Ceramic Society, Inc., 1964.

2. A. Horvath, "Physikalisch-Chemische Berechnungen in der Metallurgie" (Physico-chemical calculations in metallurgy), Akadémiai Kiadó, Verlag der Ungarischen Akademie der Wissenschaften, Budapest 1970.
3. Y. Kojima, H. Sakao, K. Sano, "Chromoxyd im Gleichgewicht mit Eisen-Chrom-Legierungen bei 1600°C" (Chromium oxide in equilibrium with iron-chromium alloys at 1600°C), Arch. Eisenhüttenwes, 39, 187, 1968.
4. H. Knüppel, "Desoxydation und Vakuumbehandlung von Stahlschmelzen" (Desoxidation and vacuum treatment of steel melts), Verlag Stahleisen m.b.H., Düsseldorf, 1970.
5. Brockhaus ABC Chemie, VEB Brockhaus Verlag Leipzig (Publisher), 1966.
6. Aurél Horváth, "Physikalisch-chemische Berechnungen in der Metallurgie" (Physico-chemical calculations in metallurgy), Akadémiai Kiadó, Budapest, 1970.
7. M.T. Farmer, et al., "MACE Test M3b, Data Report," MACE-TR-D13, Vol. 1/2; Argonne Nat. Lab., Nov. 1997
8. M.T. Farmer, et al., "MACE Test M4, Data Report," MACE-TR-D16; Argonne Nat. Lab., Aug. 1999.

Table 19-332-1—Characteristics of 1D MCCI Tests and Temperature Data

[ ]

Figure 19-332-1—Phase diagram ZrO_2-MgO

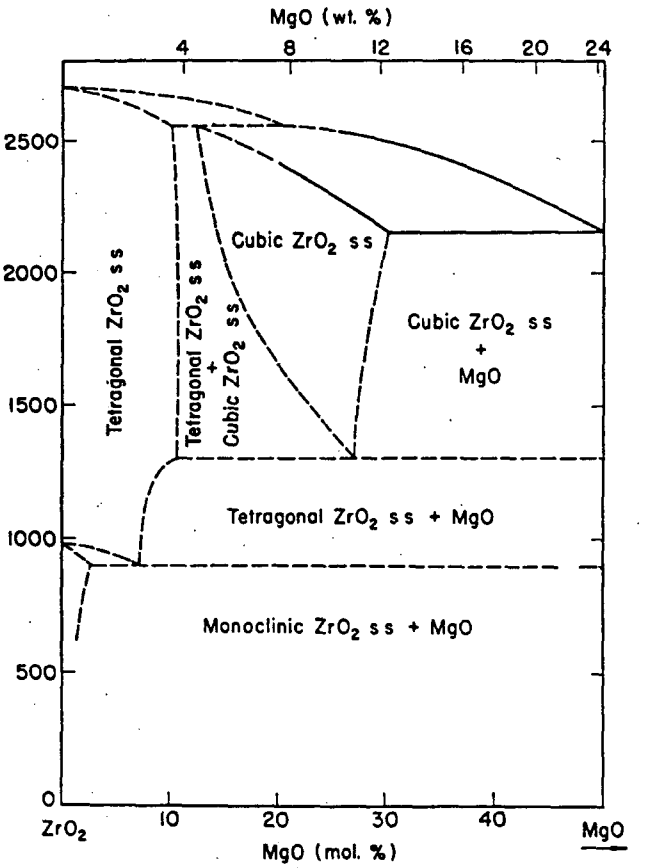

FIG. 271.—System MgO–ZrO_2; tentative.

Pol Duwez, Francis Odell, and Frank H. Brown, Jr., *J. Am. Ceram. Soc.*, **35** [5] 109 (1952).

Notes:

1. Taken from Reference 1.

Figure 19-332-2—Vertical Cross-Section of Ceramic ZrO_2 Specimen (#3004, ZIRCOA) After Interaction with Corium Melt in Experiment #27.

Figure 19-332-3—Vertical Section through Cylindrical ZrO_2 Specimen from CIRMAT "Test #24"

Figure 19-332-4—Interaction Zone of Test #24 (Schematic Representation)

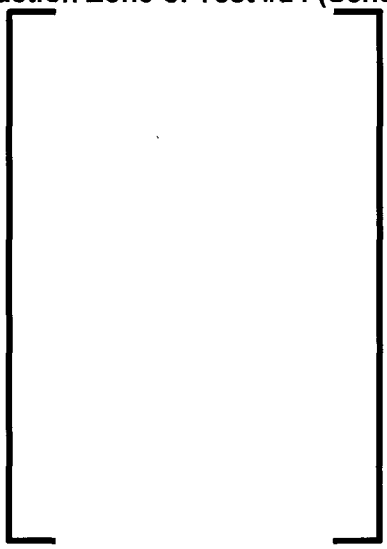

Figure 19-332-5—Oxygen Solubility in an Iron/Chromium Melt

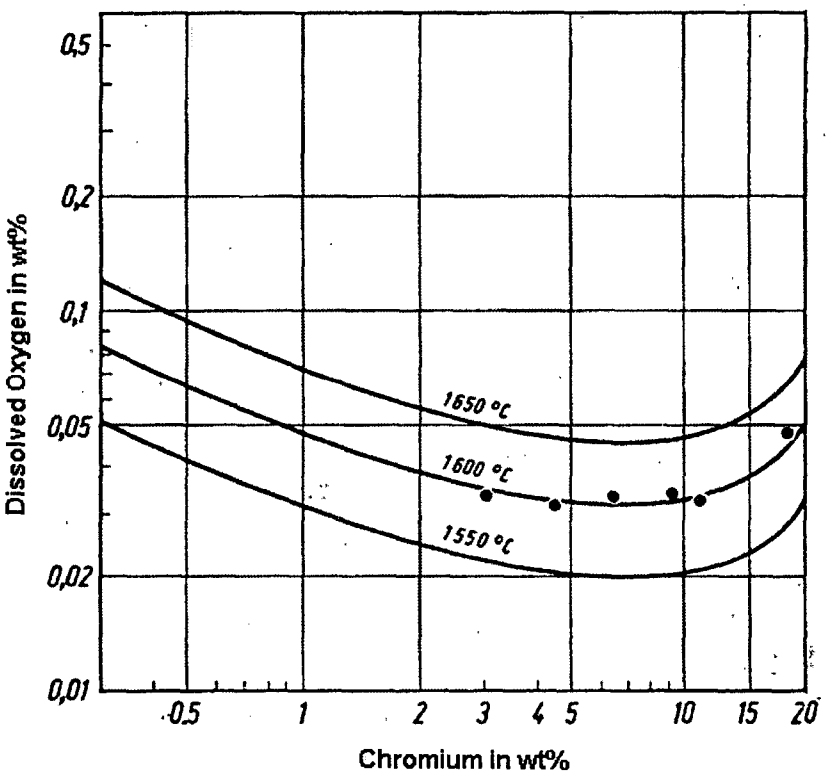

Notes:

1. Derived from Reference 4.
2. Y axis: Oxygen content in w%.
3. X axis: Chromium content in wt%.

Figure 19-332-6—Cross Section of MgO-stabilized Zirconia (#3001) Crucible after Interaction with Steel Melt (88 wt% Fe, 5 wt% Cr, 7 wt% Ni) for 6 Hours at 2200°C

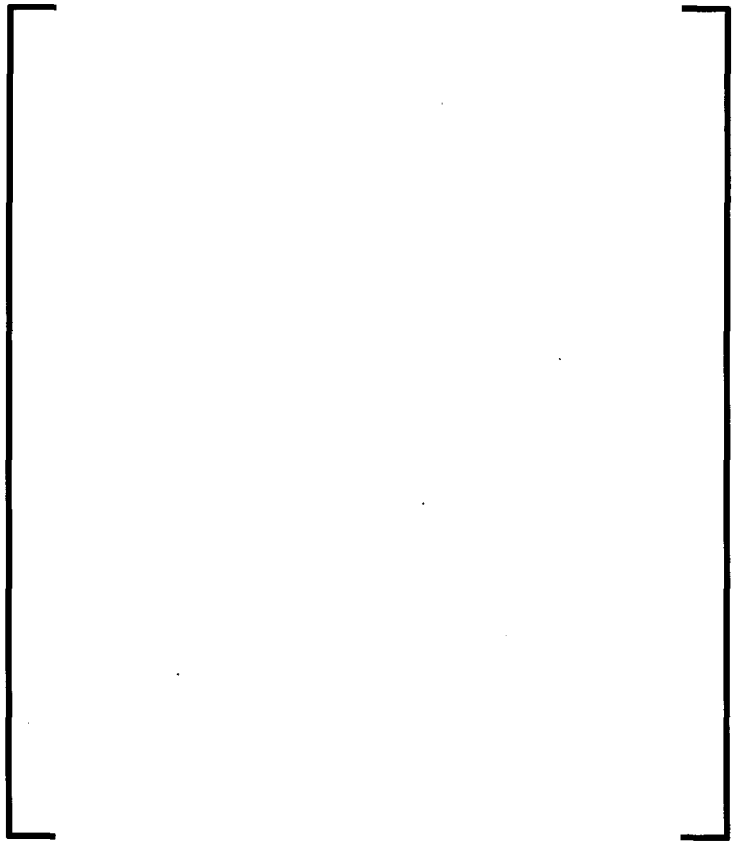

Figure 19-332-7—Scanning Electron Micrograph of Zirconia (#3001) Crucible Wall after Interaction with Steel Melt (88 wt% Fe, 5 wt% Cr, 7 wt% Ni) for 6 Hours at 2200°C

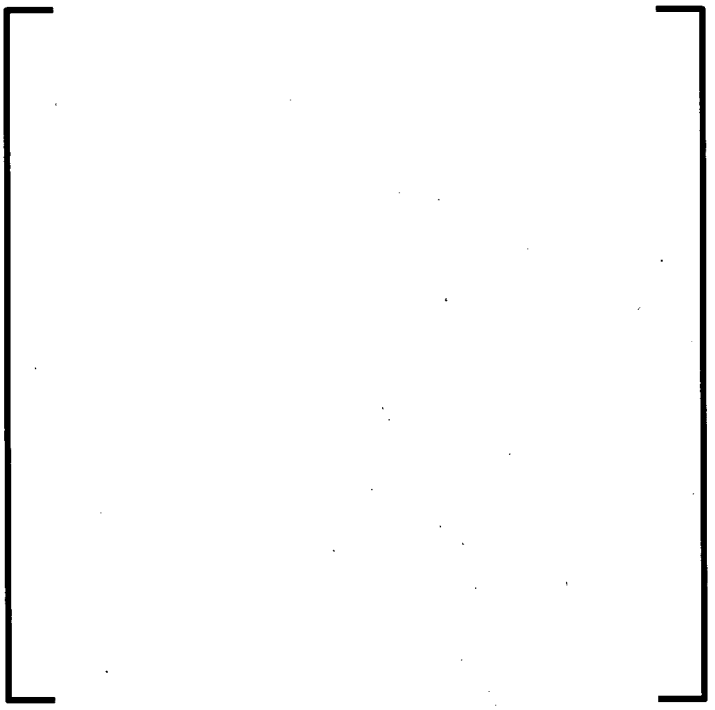

Figure 19-332-8—Scanning Electron Micrograph of Zirconia Crucible Wall before Test (Sintered Ceramic Brick, Composition #3001, ZIRCOA, as-delivered)

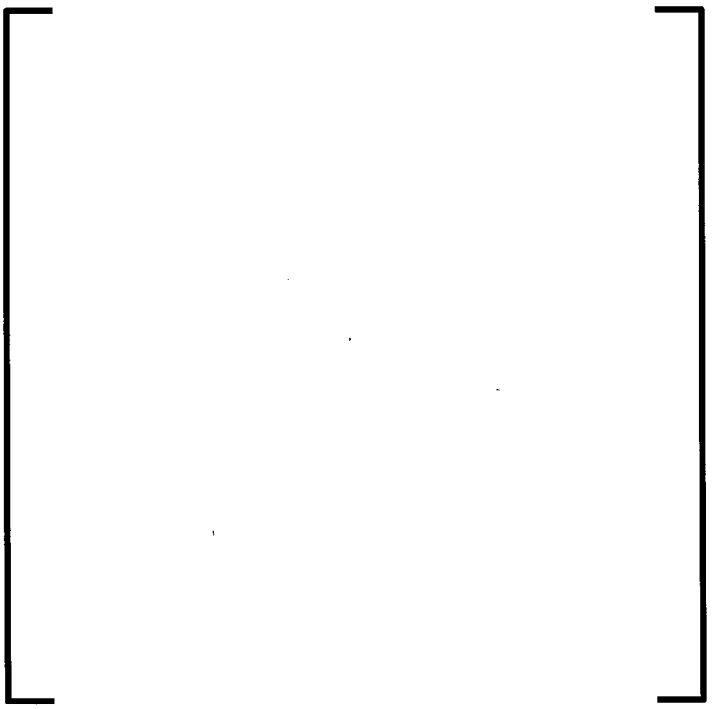

Figure 19-332-9—Scanning Electron Micrograph of Zirconia Crucible Wall before Test (Sintered Ceramic Brick, Composition #3001, ZIRCOA, as-delivered)

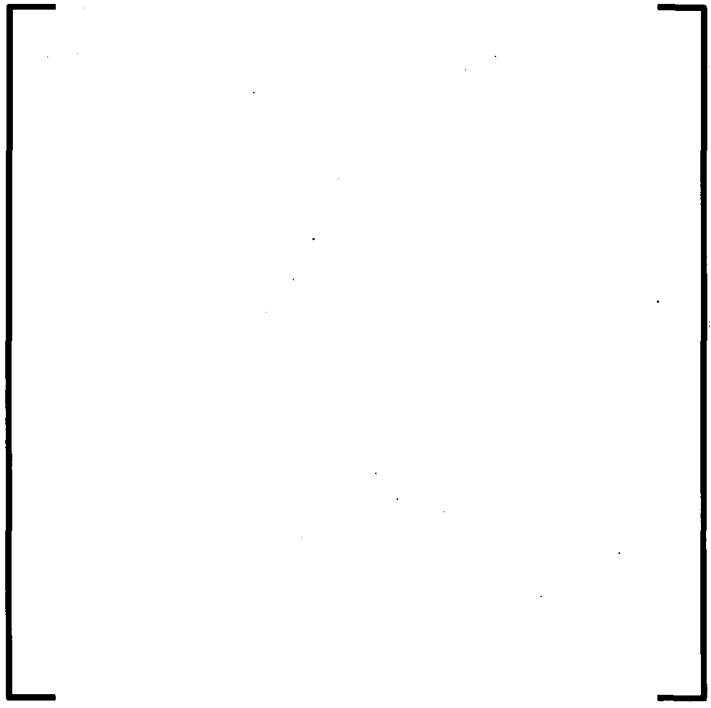

Figure 19-332-10—Temperature in the Steel Sample (Solid Block and Melt) and Oxygen Concentration in off-gas during Zirconia Test S6

Figure 19-332-11—Test S6: Cross Section of MgO-stabilized Zirconia Crucible after Interaction with Oxygen-saturated Steel Melt (88 wt% Fe, 5 wt% Cr, 7 wt% Ni) for 3 Hours at 1900°C.

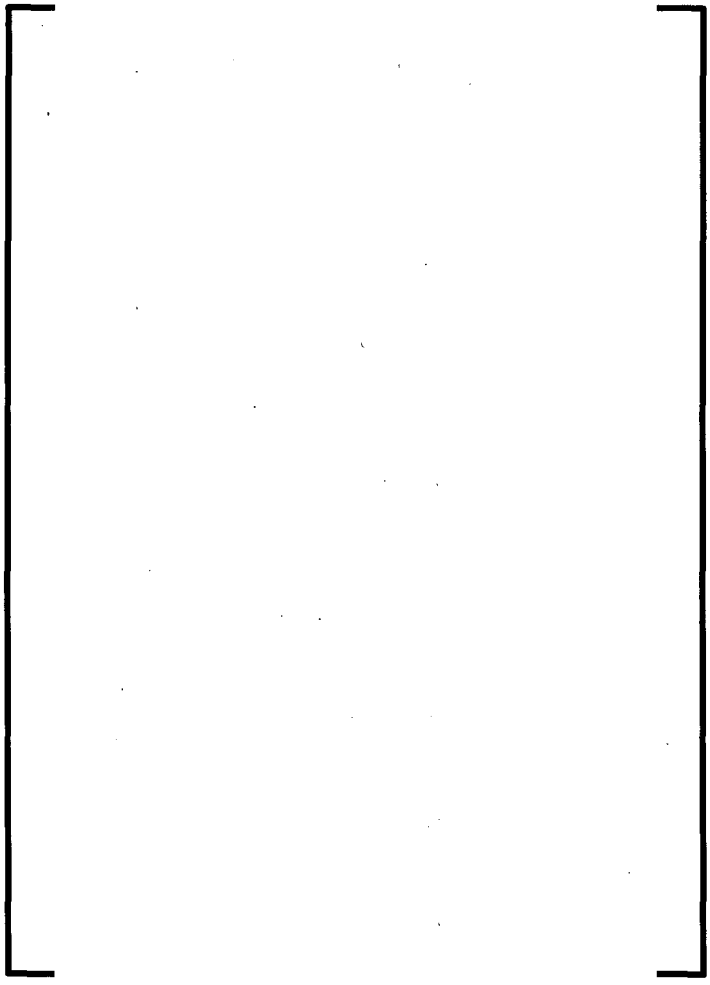

Figure 19-332-12—Temperature in the Steel Sample (Solid Block and Melt) and Oxygen Concentration in off-gas During Zirconia Test S7

Figure 19-332-13—Test S7: Cross Section of MgO-stabilized Zirconia Crucible after Interaction with Oxygen-containing Steel Melt (88 wt% Fe, 5 wt% Cr, 7 wt% Ni) for 3 Hours at 1900°C

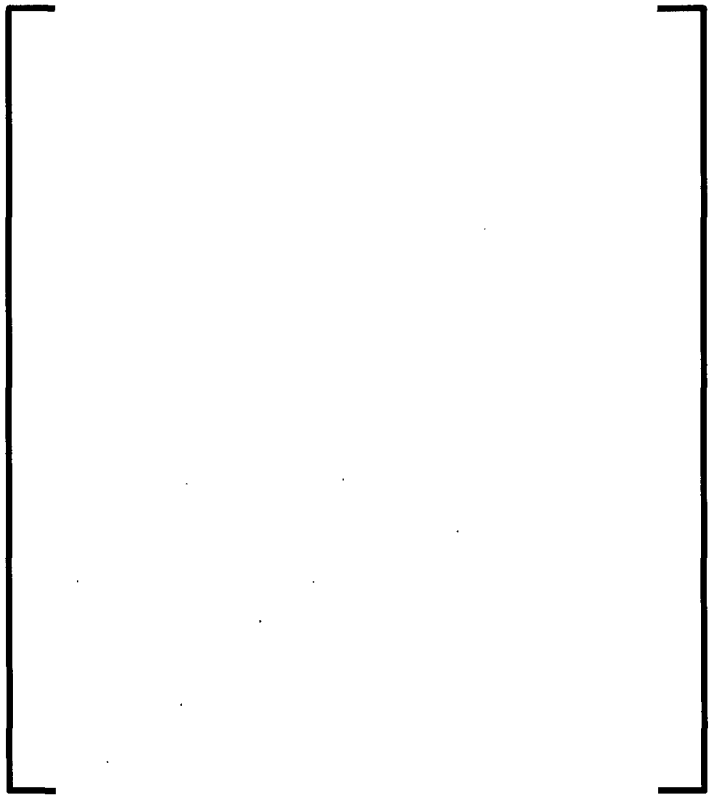

Figure 19-332-14—Experimental Temperature Profile during Total Test Duration (Heatup and Cooldown)

[ ]

Figure 19-332-15—Experimental Temperature Profile during the First 5 Hours of the Test

5

Figure 19-332-16—Experimental Temperature Profile during the First Half Hour of the Test

Figure 19-332-17—Experimental Temperature Profile during the First 200 Seconds of the Test

Figure 19-332-18—Maximum Temperatures Measured by Thermocouples at Different Locations below Zirconia Surface

[ ]

Figure 19-332-19—Calculated Course of Temperatures inside the Zirconia Layer after Metal Melt Contact (T= 1650°C) with High Effective Heat Transfer (Various Postulated Impact Times)

Figure 19-332-20—Estimated Course of Melt Pool Temperatures Assuming an Isotropic Heat Flux Equal to the Best-fit for the First Thermocouple (5 mm depth)

Figure 19-332-21—Calculated Course of Temperatures inside the Zirconia for the Course of Surface Temperatures Represented by "T_melt" in Figure 19-332-20

Figure 19-332-22—Measured Melt Temperatures in MACE 3b

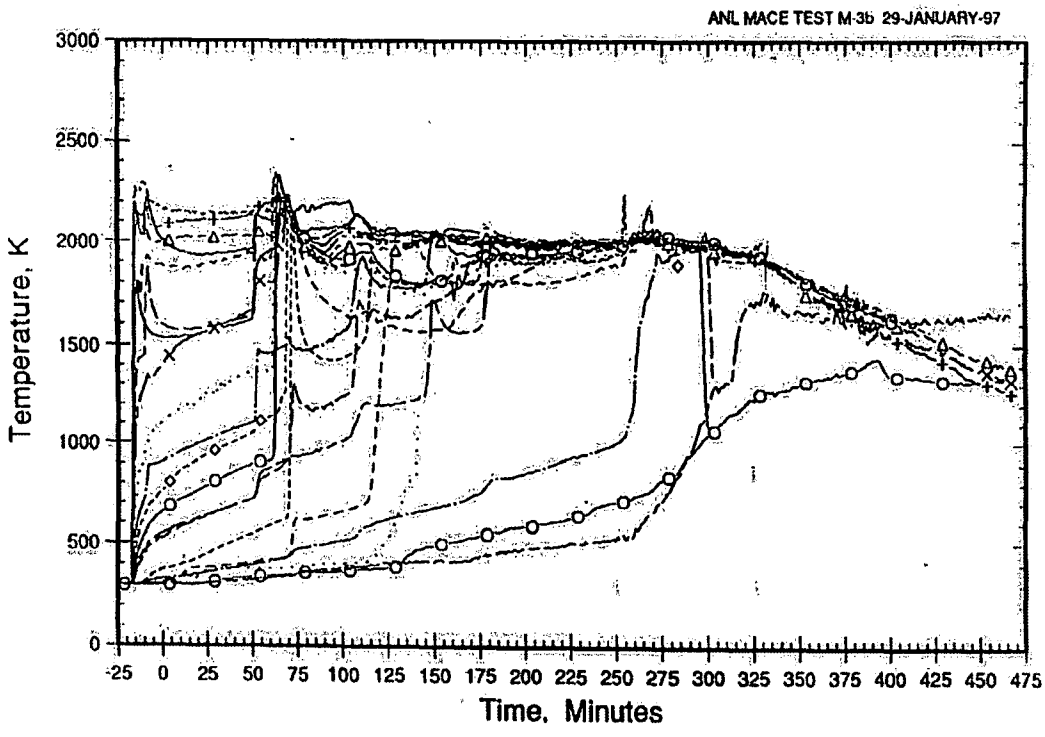

Notes:

1. MACE Test M3b Data Report Vol. 1, MACE-TR-D13, ANL Nov. 1997.

Figure 19-332-23—Measured Melt Temperatures in MACE 4 MACE Test M4 Data Report, MACE TR-D16, ANL, August 1999

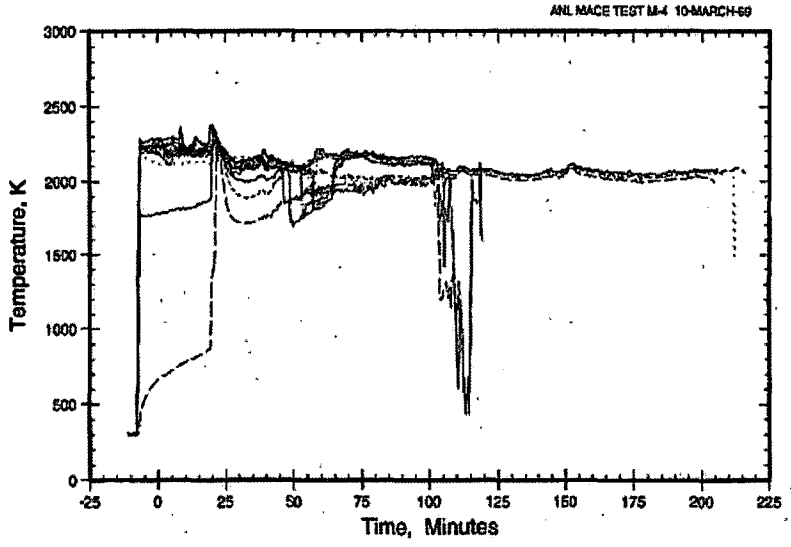

Figure 3-11. Composite Plot of All Melt Temperature Thermocouples Located Above the Concrete Initial Surface Location.

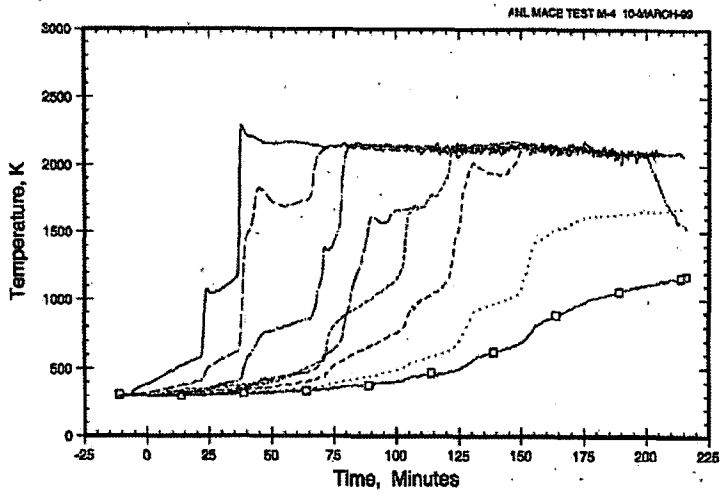

Figure 3-12. Composite Plot of All Melt Temperature Thermocouples Located Below the Concrete Initial Surface Location.

Notes:

1. MACE Test M4 Data Report, MACE TR-D16, ANL, August 1999.

Figure 19-332-24—ECOSTAR Pretest - Signals of WRE-W Thermocouples

Figure 19-332-25—Test MT 7-09 - Signals of WRE-W Thermocouples and Calculated Liquidus Temperatures

[ ]

Figure 19-332-26—Test MT 7-09 – Pyrometer Signals

Figure 19-332-27—Test C3-1 - Signals of WRe-W Thermocouples

Figure 19-332-28—Test C3-1 – Pyrometer Signal at 2 cm Concrete Ablation

Figure 19-332-29—Test A10 - Signals of WRe-W Thermocouples

Figure 19-332-30—Test A11 - Signals of WRe-W Thermocouples and Dip-in Thermocouple (WRe-W from ELECTRONITE; blue)

Figure 19-332-31—Test A2 - Pyrometer Signals

Figure 19-332-32—Test Y´ - Pyrometer Signal at 2.5 cm Concrete Ablation

Figure 19-332-33—Test OX-1 - Pyrometer Signal at 4 cm Concrete Ablation

Figure 19-332-34—Set-Up of Wedge-Splitting Test

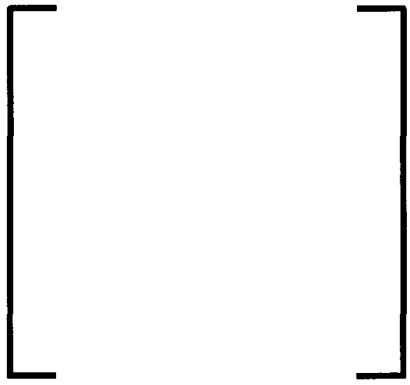

Figure 19-332-35—Force-Displacement Diagram Zettral 95gr

Figure 19-332-36—Stress vs. Non-Elastic Strain at 1500°C

Question 19-333:

OPEN ITEM

Follow-up to RAI 22, Question 19-158

The response to Question 19-158 is, for the most part, satisfactory. However, it does not address the risk implications of enhanced Ru release, especially, relative to the early and latent fatality safety goals. Please include a discussion on air ingression and enhanced release of Ru in the FSAR. In addition, please provide sensitivity calculations on the potential impact of increased Ru releases on the early and latent fatalities, and discuss impacts on the U.S. EPR SAMDA evaluation.

Response to Question 19-333

This response is divided into two parts. The first part of the response describes the phenomenon of air ingression and enhanced release of Ruthenium (Ru) in the U.S. EPR. The second part provides the results of the sensitivity calculations performed to assess the potential impact of increased Ru releases on the early and latent fatality results and discusses the impacts on the U.S. EPR severe accident mitigation design alternatives (SAMDA) evaluation.

Part A:

Air ingression Accident Scenarios for the U.S. EPR and their Relation to Ru Releases

Accident scenarios developed for the U.S. EPR include a full range of postulated accident and failure states with the potential to release fission products to the environment following fuel damage. Included in these accidental release categories are air ingression scenarios. The introduction of air into the reactor pressure vessel (RPV) in the presence of fuel damage states has been postulated to result in the increased or enhanced formation of Ru compounds. For the U.S. EPR, these accident release categories are identified in Table 19-333-1 and include the breach or rupture of the RPV or the break in the reactor coolant system (RCS).

Results from the modular accident analysis program (MAAP) analyses of the accident release scenarios show increases in the release fraction group containing Ru following the establishment of an air ingression pathway. Figure 19-333-1 is a U.S. EPR release scenario that demonstrates a period of increased Ru formation. During these periods of air ingression, the chemical equilibrium and mass transport models within MAAP simulate the generation, transformation, and transport of the formation of the Ru through the accident analysis. Ru contained within the core is model in its elemental form and is treated as RuO_2 in the release fraction FREL(5). The release dynamics for Ru are dominated by oxygen concentration, fuel surface area, and fuel temperature, of which MAAP's predictive capability is applicable. The effect of Ru during air ingression accident scenarios is captured in the release fraction results generated with MAAP. Further oxidation of RuO_2 into the highly volatile RuO_4 species is not modeled by MAAP.

An evaluation of Ru and other select fission products (CsI and TeO_2) during accident scenarios with potential for air ingression show that the containment environments are not oxygen limited and minimal retention of these fission products is seen in the lower plenum debris bed material.

These findings indicate that the oxidation and release of fission products are not limited, and the fission product species are released from the core and core debris.

Part B:

Sensitivity Calculations the Impact of Increased Ru Releases on Early and Latent Fatalities, and on the U.S. EPR SAMDA evaluation.

AREVA NP performed a sensitivity evaluation to assess the impact of enhanced Ru releases on the early and latent fatality risk calculated for the U.S. EPR, and evaluated the impact of these sensitivity calculations on the U.S. EPR severe accident mitigation design alternative (SAMDA) evaluation.

AREVA NP examined quantification and the source term results of the Level 2 at-power and shutdown probabilistic risk assessment (PRA) analyses. AREVA NP determined that the risk impact of increased Ru release would be assessed by comparing the results of the U.S. EPR Level 3 PRA to a pair of sensitivity analyses.

In the first sensitivity case (F3), a multiplication factor of three was applied to the release fractions for the MACCS2 radioisotopic group containing Ru for each of the release categories, regardless of whether air ingression pathways and enhanced Ru production are expected to form. In the second sensitivity case (F10), a factor of ten was applied to release fractions for the MACCS2 radioisotopic group containing Ru for each of the release categories, regardless of whether air ingression pathways and enhanced Ru production are expected to form.

AREVA NP judged that a bounding sensitivity analysis would be obtained by increasing the release fraction for the MACCS2 radioisotopic group containing Ru, because this group also contains molybdenum, technetium, and rhodium. Increasing the release fraction of MACCS2 radioisotopic group containing Ru increases the contribution of the radioisotopes within that fission product group. This will bound the consequences of the hypothetical increased Ru releases. AREVA NP applied the multiplication factor to the release categories, regardless of whether air ingression was likely to occur during the accident scenarios leading to the release categories.

AREVA NP judged that the request for latent fatalities in this question is adequately addressed by the consequence metric of latent cancers estimated by MACCS2.

B.1:

The Impact of Increased Ru Releases on Early and Latent Fatalities

Table 19-333-2 summarizes the results of the base case, sensitivity case F3, and sensitivity case F10 for the risk of early and latent fatalities per year at 50 miles. Table 19-333-2 provides the total early and latent fatality risk from the release categories for each sensitivity case. The process of increasing the Ru release fraction by an order of magnitude results in an increase in the risk of early fatalities. Despite the relative magnitude of the increase in these sensitivity cases, the absolute values of early fatalities remains low, so the magnitude impact on the risk from early fatalities remains small.

The risk of latent cancers is more of a time-integrated effect than the risk from early fatalities. The risk is more evenly distributed across the release categories, and the impact of increased Ru release fractions is more gradual than the impact of early fatalities.

Table 19-333-3 presents the body dose (person-rem/yr) and economic impact ($/yr) estimates at 50 miles used to evaluate the impact of enhanced Ru on the results of the SAMDA analysis.

B.2:

The Impact of Increased Ru Releases on the U.S. EPR SAMDA Evaluation

For any SAMDA candidate to be cost-beneficial for the U.S. EPR design, the implementation cost of the design alternative must be less than the cost-benefit estimated for the alternative.

This portion of the analysis estimates the cost-benefit for the two sensitivity cases, F3 and F10. It compares the cost-benefit of a hypothetical design change in each case with the implementation cost of the design change to determine if the design change would be cost-beneficial.

For this analysis, the same methodology described in the base case of Topical Report ANP-10290, "AREVA NP Environmental Report – Standard Design Certification" (Reference 1) was used to estimate the cost-benefit for the sensitivity cases F3 and F10.

Table 19-333-4 provides the total cost-benefit (including contributions from internal events, internal floods, internal fires, and seismic) for sensitivity cases F3 and F10. Reference 1 determined that the SAMDA candidate with the lowest implementation cost for any of the SAMDA candidates was candidate CW-22, with a cost of implementation of $150,000. This cost exceeds the total cost-benefit estimated for Cases F3 or F10.

Because the total benefit value from the F3 and F10 sensitivity cases do not exceed the cost of implementing a design change, the conclusions of the SAMDA analysis in Reference 1 are not affected.

B.3:

Impact of Shutdown States on the Results of the MACCS2 Sensitivity Runs

AREVA NP assessed the contribution of shutdown states to the results of the Level 3 PRA by examination of the results of the at-power Level 3 PRA and analysis of the release category frequency and source term results of the shutdown Level 2 PRA. Review of the at-power Level 3 PRA results showed that the significant contributors to the risk factors of early and latent fatalities, whole body dose, and economic impact are release categories RC206, RC304, RC404, RC701, RC702, and RC802. AREVA NP examined frequencies of these release categories in the at-power and shutdown analyses. AREVA NP determined that in the release categories except RC802, the frequency of release is dominated by the at-power results.

For RC802, a majority of the release category frequency results from the shutdown plant operating states. AREVA NP has not performed a calculation of offsite consequences for

shutdown condition, so the impact of the additional frequency for RC802 from shutdown conditions was assessed using the at-power consequences.

The offsite consequences were estimated by adding the at-power and shutdown frequencies for RC802, and recalculating the Level 3 base case results. When the results of the U.S. EPR base case plus shutdown RC802 are compared to the results from sensitivity Case F3 and Case F10 in Table 19-333-5, the risk from the sensitivity cases exceeds the risk from "Base case plus shutdown" by a substantial margin. AREVA NP concluded that the addition of the shutdown states would not affect the conclusions of the sensitivity analyses.

U.S. EPR FSAR Tier 2, Section 19.6.3.3.4 will be revised to reflect this description of the phenomenon of air ingression, the increased release of Ru in the U.S. EPR, and the results of the sensitivity calculations performed to assess the potential impact of increased Ru releases on the U.S. EPR SAMDA evaluation.

FSAR Impact:

U.S. EPR FSAR Tier 2, Section 19.6.3.3.4 has been revised in U.S. EPR FSAR Revision 2 as described in the response and indicated on the enclosed markup.

References for Question 19-333:

1. ANP-10290, Revision 1, "AREVA NP Environmental Report – Standard Design Certification," AREVA NP Inc., September 2009.

Table 19-333-1—Release Category Description and Air Ingression Pathways

Release Scenarios		Potential Air Ingression Pathways
Run ID	**Description**	
RC 101	SBO with 0.6-inch break with Containment Intact	Rupture in hot leg; vessel breach
RC 201	LOOP 0.6-inch break with diesels and melt retained in vessel	Rupture in hot leg
RC 202	SBO with 0.6-inch break, with containment spray, without debris flooding	Vessel breach
RC 203	SBO with 0.6-inch break without containment spray, without debris flooding	Vessel breach
RC 204	SBO with 0.6-inch break with containment spray, with debris flooding	Vessel breach
RC 205	SBO with 0.6-inch break, without containment spray, with debris flooding	Vessel breach
RC 206	SBO with 0.6-inch break, with containment spray, without debris flooding	Rupture in hot leg; vessel breach
RC 301	SBO with 0.6-inch break without containment spray, without debris flooding	Vessel breach
RC 302	SBO with 0.6-inch break with containment spray, with debris flooding	Vessel breach
RC 303	SBO with 0.6-inch break, without containment spray, with debris flooding	Vessel breach
RC 304	SBO with 0.6-inch break without containment spray	Vessel breach
RC 401	SBO without containment spray, without debris flooding	Rupture in hot leg; vessel breach
RC 402	SBO with containment spray, without debris flooding	Rupture in hot leg; vessel breach
RC 403	SBO with containment spray, with debris flooding	Rupture in hot leg; vessel breach
RC 404	SBO without containment spray, with debris flooding	Rupture in hot leg; vessel breach
RC 501	SBO with containment spray, without debris flooding	Rupture in hot leg; vessel breach
RC 502	SBO without containment spray, without debris flooding	Rupture in hot leg; vessel breach
RC 503	SBO with containment spray, with debris flooding	Rupture in hot leg; vessel breach
RC 504	SBO without containment spray, with debris flooding	Rupture in hot leg; vessel breach
RC 602	SBO with basemat failure	Rupture in hot leg; vessel breach
RC 701	ISGTR with fission product scrubbing	Vessel breach
RC 702	ISGTR without fission product scrubbing	Vessel breach
RC 802	ISLOCA with 10-inch break without scrubbing	Vessel breach

Table 19-333-2—Results of Sensitivity Analyses for Increased Ruthenium Releases (Early and Late Fatalities)

	Base Case	Sensitivity Case F3	Sensitivity Case F10
Early Fatalities (50 miles) (/yr)	2.40E-08	1.14E-07	9.92E-07
Latent Fatalities (50 miles) (/yr)	1.15E-04	1.96E-04	4.55E-04

Table 19-333-3—Results of Sensitivity Analyses for Increased Ruthenium Releases (Whole body Dose and Economic Impact)

	Base Case	Sensitivity Case F3	Sensitivity Case F10
Whole body dose (50) (person-rem/yr)	1.81E-01	2.39E-01	4.24E-01
Economic Impact (50) ($/yr)	1.85E+02	2.31E+02	3.56E+02

Table 19-333-4—Cost Benefit Results for the Sensitivity Cases F3 and F10

	Total Benefit Point Estimate CDF	Total Benefit Mean CDF
Sensitivity Case F3	$73,630	$93,872
Sensitivity Case F10	$82,879	$102,773

Table 19-333-5—Comparison of the Impact of Shutdown RC 802 to the F3 and F10 Sensitivity Cases

Release Category	Early Fatalities (50 miles) (/year)	Latent Cancers (50 miles) (/year)	Whole body dose (50 miles) (/year)	Economic Impact (50 miles) ($/year)
EPR Base case plus Shutdown RC802	7.23E-08	1.73E-04	2.35E-01	2.17E+02
EPR Base case	2.40E-08	1.15E-04	1.81E-01	1.85E+02
Case F3	1.14E-07	1.96E-04	2.39E-01	2.31E+02
Ratio of F3 to EPR Base case plus Shutdown 802	157%	113%	102%	107%
Case F10	9.92E-07	4.55E-04	4.24E-01	3.56E+02
Ratio of F10 to EPR Baseline plus Shutdown 802	1372%	262%	181%	164%

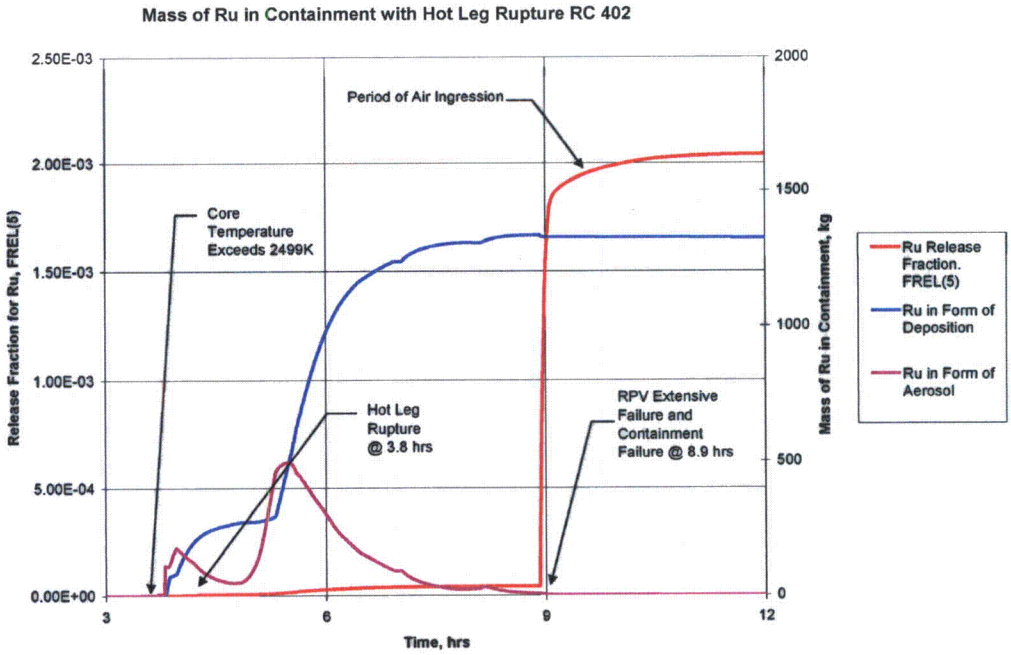

Figure 19-333-1—MAAP Analysis of Ru Release Fraction During Air Ingression

U.S. EPR Final Safety Analysis Report Markups

19.1.6.3.3.3 Source Term Evaluation

The source term associated with potential severe accident sequences identified by the Level 1 PRA occurring from an initially at-power condition is analyzed as part of the Level 2 PRA study. Tools, models, and codes available for such analysis are relatively mature; although, large uncertainties still exist with regard to certain phenomena and processes. The EPR Level 2 PRA used the MAAP 4.0.7 code to quantify the source terms associated with the at-power severe accident sequence release categories.

The codes and models available to simulate an accident occurring during shutdown have a number of limitations because they were not originally designed to simulate these conditions. Examples of such limitations are:

- Difficulties in modeling "open" RCS states (i.e., those where the RPV head is removed, and where the refueling cavity may or may not be filled).
- Modeling the effects of air ingress during the event.

The approach adopted in this U.S. EPR PSA2 shutdown study is a simplified approach for estimating shutdown source terms that addresses the specific aspects of shutdown conditions judged as most important.

This approach uses the results from a set of MAAP runs that were performed specifically for the shutdown state. Source terms for the intact containment and for a 1-meter square containment failure at time zero were evaluated for POS CA and CB using MAAP. The results of these MAAP runs were combined with the results from the at-power analysis and modifications were made based on insights from sensitivity studies performed during the analysis of at-power source terms. These modifications include decontamination factors due to containment sprays for MAAP each fission product group, and a multiplication factor for the source term that is calculated assuming no fission product retention in the primary system.

The results of the shutdown source term analysis for each of the Plant Operating States are contained in Table 19.1-113, Table 19.1-114, and Table 19.1-115.

19.1.6.3.3.4 Air Ingression

19-333

During accident scenario progression, the introduction of air into the damaged reactor core (air ingression) can further facilitate the oxidation of fuel. Some fission product releases, such as ruthenium (Ru), can be enhanced by the air ingression-induced fuel oxidation forming volatile Ru oxides (RuO_x) of radiological importance.

Air ingression scenarios with potential applicability to the EPR include:

1. Vessel Failure – Accidents where the RPV fails and air is drawn up into the vessel passing over the overheated fuel matrix.

19-333

2. Line Rupture – Breaks in the RCS line that allows air to be drawn down into the RPV and across the overheated fuel matrix.

3. Refueling Operations – Loss of coolant accident during refueling operations when the fuel handling when the RPV head is removed and the water level drops allowing the fuel to become exposed to air in the atmosphere.

During an EPR vessel rupture or breach, air ingression can occur when a failure in the lower vessel opens an air pathway upwards into the lower region of the core. Air can contact the overheated, damaged fuel in the reactor core. Similarly, a break or rupture in a portion of the RCS piping can open an air ingression pathway drawing air down through the RPV and allowing contact with fuel matrix in the reactor core. Both of these scenarios have the potential to generate high convective air flows through the core material and produce an environment of increased oxidation potential adjacent to the fuel matrix. These air ingression scenarios are analyzed in the EPR Level 2 with the impact evaluated in the EPR Level 3.

During shutdown refueling operations, the potential to establish an air ingression pathway exists when head had been removed and fuel is either in place or being moved. A rupture or breach of the vessel or other failure that results in the loss of coolant can cause the fuel to become uncovered. Without adequate cooling, the fuel can become overheated and fail. In this scenario, the fuel is oxidized when exposed to air in the atmosphere. This air ingression scenario is addressed in the EPR Shutdown Level 2.

Due to the increased oxidation associated with the air ingression scenarios, the formation of RuO_x compounds becomes a related effect. The contribution of the increased RuO_x in the releases from air ingression accident scenarios is determined by MAAP analysis and is represented in the EPR Level 2 source term results. Ruthenium is present in the fuel as elemental Ru and is transformed to its form as RuO_2 in the fission product releases. Once the primary system or reactor pressure vessel has been breached, the Ru transport and release is phenomenologically characterized as RuO_2. Modeling of air ingression release scenarios is performed using the MAAP chemical transformation, equilibrium, reaction kinetics, aerosol and deposition rates, transport processes and other process variable applications from the existing subroutines and parameters to simulate air flow and oxidation rates. Further oxidation of RuO_2 into the highly volatile RuO_4 species is not modeled by MAAP; however, the total mass of Ru released from the fuel is not affected by this modeling decision.

Results of sensitivity analyses has shown that enhanced RuO_x formation does increase the risk of early fatalities, but does not change the conclusions of the SAMDA analysis contained in the U.S. EPR Environmental Report (Reference 59).

39. NUREG/CR-0098, N. M Newmark and W. J. Hall, "Development of Criteria for Seismic Review of Selected Nuclear Power Plants," U.S. Nuclear Regulatory Commission, May 1978.

40. EPRI TR-102266, "Pipe Failure Study Update," Electric Power Research Institute, 1993.

41. NUREG/CR-2300, "A Guide to Performing Probabilistic Risk Assessment of Nuclear Power Plants," U.S. Nuclear Regulatory Commission, 1983.

42. RES/OERAB/SO2-01, "Fire Events–Update of U.S. Operating Experience, 1986-1999," commissioned by the Office of Nuclear Regulatory Research, January 2002.

43. NUREG/CR-6928, Eide, S.A., et al. "Industry-Average Performance for Components and Initiating Events at U.S. Commercial Nuclear Power Plants," U.S. Nuclear Regulatory Commission Report, February 2007.

44. NUREG-1829, Tregoning, R., et al., "Estimating Loss-of-Coolant Accident (LOCA) Frequencies Through the Elicitation Process," U.S. Nuclear Regulatory Commission Report–Draft Report for Comment, June 2005.

45. NUREG/CR-6365, MacDonald, P.E., et al. "Steam Generator Tube Rupture Failures," U.S. Nuclear Regulatory Commission Report, April 1996.

46. NUREG/CR-6595, Appendix A, Rev 1, "An Approach for Estimating the Frequencies of Various Containment Failure Modes and Bypass Events," U.S. Nuclear Regulatory Commission, 2004.

47. NUREG-1524, "A Reassessment of the Potential for an Alpha-Mode Containment Failure and a Review of the Current Understanding of Broader Fuel Coolant Interaction Issues: Second Steam Explosion Review Work Group Workshop," U.S. Nuclear Regulatory Commission, 1996.

19-333

48. Deleted.

49. Deleted.

50. Deleted.

51. Deleted.

52. Deleted.

53. ANP-10309P, Revision 0, "U.S. EPR Digital Protection System Technical Report," AREVA NP Inc., November 2009.

54. EMF-2110(NP)(A), Revision 1, "TELEPERM XS: A Digital Reactor Protection System," Siemens Power Corporation, July 2000.

55. IEC-62340, "Nuclear Power Plants – Instrumentation and Control Systems Important to Safety – Requirements to Cope with Common Cause failure (CCF)," Edition 1.0, International Electrotechnical Commission, 12-7-2007.

56. IEC-60880, "Nuclear Power Plants – Instrumentation and Control Systems Important to Safety – Software Aspects for Computer-Based Systems Performing Category A Functions," Edition 2.0, International Electrotechnical Commission, 5-9-2006.

57. IEC-61508, "Functional Safety of Electrical / Electronic / Programmable Electronic Safety-Related Systems," International Electrotechnical Commission.

58. ANP-10304, Revision 1, "U.S. EPR Diversity and Defense-in-Depth Assessment Technical Report," AREVA NP Inc., December 2009.

19-333

59. ANP-10290, Revision 1, "Environmental Report Standard Design Certification," AREVA NP Inc., September 2009.